Materiales de Construcción 75 (359)
July-September 2025, e382
ISSN-L: 0465-2746
https://doi.org/10.3989/mc.2025.387024

Evaluation of superabsorbent polymer in low water-to-cement ratio cement based materials using X-Ray μCT

A. Yusuf ✉, I. Sandi Darma, E. Zulkifli, R. Pradoto

Department of Civil Engineering, Bandung Institute of Technology (Bandung, Indonesia)
✉: lieayoo.412@gmail.com

Received 11 July 2024
Accepted 16 January 2025
Available on line 11 March 2026

ABSTRACT: Superabsorbent polymers (SAP) are powdered chemical mixtures with the potential to significantly impact of cement-based materials in both fresh and hardened states. SAP's ability to absorb and release water makes it suitable for internal curing, preventing unhydrated cement, and influencing the hydration process. This study aimed to evaluate the SAP as an internal curing medium in low water-to-cement ratio cement based materials using X-Ray μCT for image processing. SAP increased the compressive strength by 17.4% due to densification within the capillary pores, evidenced by a decrease in pore peak thickness and no increase in percolated voids. In swollen state, SAP particle appears as complete circle at close to the surface and ring-like shape in the center. Furthermore, an assessment of durability was performed through capillary absorption within crack pathways. Specimen without SAP displayed a 2.7 times greater penetration than specimen with SAP, indicating a significant impact on the durability.

KEY WORDS: Superabsorbent polymer; High-strength cement based materials; Pore structure; Transport Properties; X-ray microtomography.

Citation/Citar como: Yusuf A, Sandi Darma I, Zulkifli E, Pradoto R. 2025. Evaluation of superabsorbent polymer in low water-to-cement ratio cement based materials using X-Ray μCT. Mater. Construcc. 75(359):e382. https://doi.org/10.3989/mc.2025.387024

RESUMEN: *Evaluación de polímeros superabsorbentes en materiales cementicios de baja relación agua-cemento mediante microtomografía de rayos X (μCT).* Los polímeros superabsorbentes (SAP) son mezclas químicas en polvo con gran potencial para mejorar materiales cementicios en estados frescos y endurecidos. Su capacidad de absorber y liberar agua los hace ideales para el curado interno, evitando cemento no hidratado e influyendo en el proceso de hidratación. Este estudio evaluó el SAP como medio de curado interno en materiales con baja relación agua-cemento, usando microtomografía de rayos X (μCT). El SAP aumentó la resistencia a la compresión en un 17,4% debido a la densificación de poros capilares, evidenciada por un menor grosor de poros y sin incremento en vacíos percolados. En estado hinchado, el SAP se observa como un círculo completo cerca de la superficie y un anillo en el centro. La evaluación de durabilidad mostró que las muestras sin SAP tenían 2,7 veces más penetración de agua en grietas que las muestras con SAP, destacando su impacto en la durabilidad.

PALABRAS CLAVE: Polímero superabsorbente; Materiales cementicios de alta resistencia; Estructura de poros; Propiedades de transporte; Microtomografía de rayos X.

1. INTRODUCTION

Cement-based materials are composite materials composed of cement, aggregate, water, and additives. Over time, significant advancements have been made in cement-based materials, with the introduction of supplementary cementitious materials such as fly ash and silica fume, which contributing to these materials' improved strength and durability (1).

In recent years, some research has investigated superabsorbent polymers (SAP). SAP can absorb and release water within a specified period (2). Since water plays a critical role in the formation of cement paste, the utilization of SAP has a profound impact on various properties of cement-based materials, including their rheological properties, workability, hydration process, transport properties, microstructure formation, mechanical properties, and durability. SAP as an internal curing medium involves maintaining a favourable relative humidity (3) by supplying water to the surrounding pores within a range of 2-3 mm. This process promotes continued hydration and reduces self-desiccation, enhancing mechanical properties such as compressive strength. However, the incorporation of SAP also introduces certain drawbacks, such as reduced workability and compressive strength, due to the increased macro-porosity resulting from the formation of SAP voids. The extent of strength reduction depends on the size of SAP particles, with compressive strength decreases ranging from 10-20% for SAP sizes of 300-500 μm to 30-50% for sizes of 50-150 μm (4). Furthermore, the water-to-cement ratio (w/c) and water content significantly influence the effectiveness of SAP as an internal curing medium. Previous studies have suggested that a w/c ratio of 0.2 is particularly effective in reducing porosity (5).

In addition to material innovations, there have been significant advancements in testing methods for evaluating cement-based materials. Presently, most research employs indirect testing approaches, such as assessing hydration through heat-based methods (6), evaluating porosity through techniques like mercury intrusion porosimetry (MIP) (7, 8) or scanning electron microscopy (SEM) slice cross-section (9), and quantifying capillary absorption by measuring the percentage of additional weight due to water penetration (10). However, these indirect methods are associated with certain inaccuracies; MIP has limitations in accurately to measure the pore due to the ink-bottle effect (11) and possibly to damaging the microstructure of cement-based materials (12), while SEM values were approximately 3 times higher than 3D X-Ray μCT (13). For instance, the assumption of uniform suction penetration height throughout the cross-section based solely on weight gain introduces limitations.

X-Ray μCT stands out as a non-destructive testing technique for producing accurate 3D microstructural information for evaluating cement-based materials (14, 15). This method directly assesses cement-based materials properties, such as pore thickness based on 3D imaging, hydration rate based on increased grayscale values, and capillary absorption by examining in 2D orthogonal slices. Moreover, X-Ray μCT can also assess the durability of cement-based materials by identifying the presence of cracks and liquid penetration using tracers (16). Previous research has highlighted the utility and reliability of X-ray μCT for visualizing fluid transport in cement-based materials (17, 18). This method is comparable to the conventional water absorption technique outlined in ASTM C1585. The crack geometry parameters can be characterized by analyzing crack thickness distribution, tortuosity, and constrictivity.

Therefore, this research aims to explore the influence of SAP in cement-based materials using X-Ray μCT. By employing this technique, the study aims to provide precise analysis and reliable findings regarding the effects of SAP on hydration, porosity, pore evolution, and the transport properties of cement-based materials. Moreover, the durability aspect was evaluated by performing capillary absorption of potassium iodide tracer within crack pathways.

2. MATERIALS AND METHODS

2.1. Materials

In this study, ordinary Portland cement with composition as detailed in Table 1 was used conforming to ASTM C150, quartz sand mesh 30-80 as aggregate, and a polycarboxylate high-range water reducer to improve workability of the mixtures. A superabsorbent polymer (SAP) was utilized as an internal curing medium. The SAP particles employed in this study had a particle size ranging from 100 to 200 μm. The properties of SAP were tested for absorbency and desorption rate, following the guidelines outlined by RILEM TC 260-RSC. The absorbency test conducted within 24 hours revealed that the SAP could absorb 277 grams of water per gram of SAP and 92 grams of a pH 12 solution per gram of SAP, representing the pH condition of cement-based materials (19). Subsequently, during the desorption test, it was found that the SAP could release 9% of the absorbed water within 24 hours.

Table 1. Composition of cement (%).

SiO_2	Fe_2O_3	Al_2O_3	SO_3	MgO	CaO	Loss
20.4	9.84	6.4	2.44	1.84	55.4	3.7

Table 2. Mix design.

Specimen	W/C	S/C	SAP (C x %)	HRWR (C x %)
Ref	0.2	1.0	-	7.5
SAP	0.2	1.0	0.2	9

2.2. Mixture proportion

The mixture proportions must feature a low water-to-cement ratio (w/c) with low water content to effectively observe the role of SAP as an internal curing medium. Therefore, the water to cement ratio was set to 0.2 while the sand to cement ratio was 1.0. The amount of dry SAP utilized was determined to be 0.2% by weight of the cement content, which was selected based on previous research by (20) and no additional water was added to the SAP specimens. SAP homogenization is achieved by mixing it in its dry state, allowing for thorough integration. The level of uniformity in the mixing process is comparable to that of cement and sand, making it feasible for real-world construction applications. The use of SAP absorbs mixing water, which can lead to a loss of flowability in the mixture (4). The dosage of the HRWR (High range water reducer) was adjusted to achieve comparable flow at 90%, following ASTM C1437, for both Ref- and SAP specimens. In this mix design, the use of 0.2% SAP requires an additional 1.5% HRWR to compensate for the loss of flowability. The specific mix design of cement, fine aggregate, and SAP employed in the study are presented in Table 2.

2.3. Compressive strength

Compressive strength tests were conducted on Ref-specimens and SAP-specimens using a universal testing machine, following the guidelines outlined in the ASTM C39. For each testing age (1, 3, 7, and 28 days), three specimens of cylindrical with a diameter of 102 mm and height of 203 mm. Each specimen was removed from its mold after 24 hours and cured by water curing until the age of tests.

2.4. Imaging methods and image analysis of the internal structure

The X-Ray μCT imaging system utilized in this research was located at Basic Science Center A Laboratory, Faculty of Mathematics and Natural Sciences in Bandung Institute of Technology. The system was operated under specific parameters, including a voltage of 130kV, a current of 80μA, an exposure time of 1500 ms, and a rotation step of 0.2°. These settings facilitated the acquisition of 1800 2D image slices, each with dimensions of 2240×2240 pixels and a resolution of 26 μm/pixel.

The processing of acquired 2D images using ImageJ/FIJI software, an automated and objective software tool. A square-shaped region of interest (ROI) measuring 1000×1000 pixels was selected from the central specimen in 1000 consecutive images to make a volume of interest (VOI) of 1000^3 voxels. This VOI was chosen to capture the internal structure and properties of the specimens. Various parameters related to the cement-based materials were evaluated, including the hydration rate, porosity, pore size distribution, and pore shape. For each testing age (1, 3, 7, and 28 days), one specimens of cylindrical with a diameter of 44 mm and height of 44 mm. The number of specimens was limited due to the duration of scanning, the time required for image analysis, and the overall cost of testing.

The hydration rate can be estimated by monitoring the increase in greyscale values, then visualized in a histogram. As the material density rises during the hydration process, leading to a rightward shift in the histogram distribution. The grayscale analysis was validated using X-ray imaging of water for calibration purposes (21). Noise in the images may arise due to the resolution limitations of the device. As a result, the analysis focuses on pores larger than 26 μm, as pores smaller than 26 μm fall into ambiguous regions and are less reliable for interpretation.

Pores in cement-based materials are characterized as trapped air and exhibit a lower density than the surrounding matrix. Consequently, in the resulting image, voids appear as dark-colored pixels. Pores can be visually observed by directly examining a 2D slice image in grayscale values. However, when quantifying pore thickness, specific pixels may present ambiguity about whether they should be classified as voids or matrix. Making a pixel binary is a way to ensure whether it is void or matrix. The histogram-based method (22, 23) determines void and matrix boundaries to produce a threshold value, each object was assigned a unique threshold value. Once the pores have been segmented based on the threshold value, a subsequent analysis can be conducted to extract information such as porosity, pore size, and pore shape.

The 3D volumetric method (24) has been explored to quantify porosity using Thickness BoneJ (25, 26, 27) in ImageJ. Porosity can be classified into isolated and percolated pores, depending on whether the pore is connected to the external environment or not.

Measuring thickness is one approach to determine pore size, which allows for the acquisition of pore size distribution and plotted through a histogram. Analyzing the pore thickness at different time, such as 1, 3, 7, and 28 days, provides insights into the evolution of pores. The 3D analytical capabilities of X-Ray μCT enable the determination of pore shape based on sphericity, indicating the spherical of a pore within the range of 0-1. Sphericity is classified into five categories: pipe, elongate, low, moderate, and high (28).

2.5. Volume of permeable void

Volume of permeable void tests were carried out in accordance with ASTM C642 on specimens aged 28 days. Cylindrical specimens with a diameter of 102 mm and a height of 203 mm were employed for this testing. Water

penetration resulting from immersion in water and the boiling process was assumed represent the true porosity of the specimens, serving as a calibration for the X-Ray μCT porosity method.

2.6. Capillary absorption

The capillary absorption test, in accordance with ASTM C1585 and following the schematic outlined by (16), was conducted in this study. Before the test, the lateral side of the specimen was sealed using a heat shrink tube. The bottom surface of the specimen was submerged by approximately 2 mm in tracer solution to enhance the X-Ray attenuation of water in the CT images.

A tracer substance with a different density than the voids was utilized to enhance visualization of the penetration height. This approach leverages the principle that the X-ray μCT imaging system operates based on the object's density, determined by the attenuation of neutrons after penetrating the material. At a constant power (kV), denser and thicker objects yield lower-quality images. Various solutions have been commonly employed as tracers, including Cesium Carbonate (Cs_2CO_3) (16), Cesium Chloride (CsCl) (29), and Potassium Iodide (KI) (30, 31). In this study, Potassium Iodide (Merck 1.05043) was selected as the tracer due to its resemblance to Cesium in terms of chemical properties (both belonging to the same major group in the periodic table of elements) (29). Furthermore, iodide has a similiar concentration profile to chloride (31).

The uptake of water can be determined from the 2D orthogonal slices, and the capillary coefficient can be calculated as follows:

$$x = kt^{1/2} \qquad [1]$$

where x is the height penetration of water uptake (m) and k is the capillary coefficient ($m/s^{1/2}$).

Testing capillary absorption from the bottom surface raises concerns, particularly due to the smoothness of the surface resulting from the cutting process. Additionally, cutting can damage the microstructure, making it unrepresentative for evaluating transport properties. To address these limitations, capillary absorption testing through cracks is proposed, allowing lateral penetration into the specimen to better simulate real conditions. This method aims to provide a more accurate assessment of transport properties.

The capillary absorption through crack test is the same as ordinary capillary absorption, but a crack needs to be created first through the splitting/brazillian test. The cracked specimens were stabilized using heat-shrinkable tubing applied beforehand, a setup that was established in a previous study (16). Five specimens per mix were tested to ensure that only a single, straight crack was produced, avoiding any branching cracks. The image processing conducted on a cube-shaped VOI of 500^3 voxels, selected from the central area within the specimen. This VOI is used to monitor the penetration of the tracer through the crack in the lateral direction. Then, the crack geometry parameters are extracted from the 3D images, such as crack width distribution, tortuosity, and constrictivity.

2.7. Image analysis of crack geometry parameter in 3D crack space

A VOI 500^3 voxels is selected from the center of the specimen, which has been cracked through a splitting test. This VOI is then segmented through thresholding, where white represents voids and cracks. The splitting and thresholding procedures followed the method outlined by (16).

Tortuosity, representing the ratio of the crack path length to the distance between the two crack tips, is determined using the AnalyseSkeleton plugin (32), from 2D image of crack space to skeleton image of crack space so the crack width is reduced to just 1 pixel, facilitating the measurement of the tortuous crack length. A tortuosity value of 1 signifies a straight crack path between the two tips, while higher values indicate a more meander path.

Furthermore, by using crack width data, constrictivity can be evaluated (33). A constrictivity of 1 denotes uniform crack width along crack path, whereas a value below 1 signifies the presence of a gap in crack width.

2.8. SAP presence and dispersion

The mechanism of SAP, which absorbs water and gradually releases it over a certain period, as outlined by RILEM TC 260-RSC, needs to be further studied to assess the effectiveness of SAP. In order to observe the presence of SAP and its dispersion capability in terms of its effective range when releasing water as an internal curing medium, test specimens were prepared with different mix design and SAP condition, SAP in a presoaked condition using a potassium iodide 4 M as a tracer. In addition to increasing the molarity of the tracer, reducing the density of the cement-based material can enhance image clarity, enabling a more precise evaluation of of SAP presence and dispersion capability within the material. With these considerations, the mixture was designed with a water-to-cement ratio (w/c) 0.5 to lower the density of the mortar and enhance the clarity of images of SAP in the pores. X-Ray μCT scanning was carried out at 1, 3, and 7 days to observe the SAP particles and their dispersion. The analysis focused on a specific void within a volume of interest (VOI) of 120×120×60 voxels.

3. RESULTS AND DISCUSSION

3.1. Compressive strength

Figure 1 shows the growth of compressive strength over time. On day 1, the compressive strength of SAP-specimens is lower compared to Ref-specimens. SAP's ability to absorb water contributes to reducing the amount of water used for the hydration process. The presence of SAP not only reducing the amount of water but also increasing total pores. The SAP-filled water might be defined as void, increasing total pores in the mortar, resulting in lower compressive strength.

Furthermore, starting from day 3, the compressive strength of SAP specimens surpasses that of Ref-specimens. After 24 hours, SAP can release as much as 9% water. Water supply from SAP could enhance the hydration process in the latter ages. The study conducted by (34) stands as the sole prior research that observed a higher compressive strength of SAP-specimens compared to Ref-specimens in the time range of 7 to 14 days with amount of SAP 0.1% by weight of binder. However, insufficient supporting data available to confirm this increase in compressive strength during the 7 to 14 days timeframe. Previous studies analyzing cumulative heat did not identify occurrences of overcoming within the 7 to 14 days timeframe.; (35) observed such behavior within 14-24 hours, while other study (36) reported it around the 20-hour.

Notably, the previous state-of-the-art report reveals that significant increases in compressive strength resulting from SAP usage are infrequent because of strength reduction due to macro void formed by SAP (37). In addition, strength reduction may occur due to the use of extra water, often referred to as Wic (internal curing water) (7, 8). Extra water is typically added to compensate for the loss of workability caused by the water absorbed by SAP. However, in this study, a high-range water reducer (HRWR) was used to maintain workability and prevent the need for extra water.

Only a limited number of previous studies have reported an enhancement in the compressive strength of SAP-specimens compared to Ref-specimens. For instance, (38) reported a 15% increase at the 28-day mark using an SAP dosage of 0.5% by weight of the binder, but this study did not explore the observation of hydration and compressive strength growth. Additionally, (32) observed around a 12% increase at 60 days, employing an SAP dosage of 0.1% by weight of the binder.

A fascinating phenomenon was discovered when observing the crushed mortar surface following the compressive strength test at 28-day. As seen in Figure 2, the crushed surface for Ref-specimens resembles cement powder which is expected unhydrated cement. Meanwhile, SAP-specimens revealed a typical surface of hardened cement based materials. In this regard, SAP specimens with low W/C shows higher final degree of hydration compared to that of Ref-specimens.

This study, however, observed an 17,4% enhancement in compressive strength for SAP-specimens while keeping key variables such as water content, water-to-cement ratio (w/c), workability, and compaction consistency.

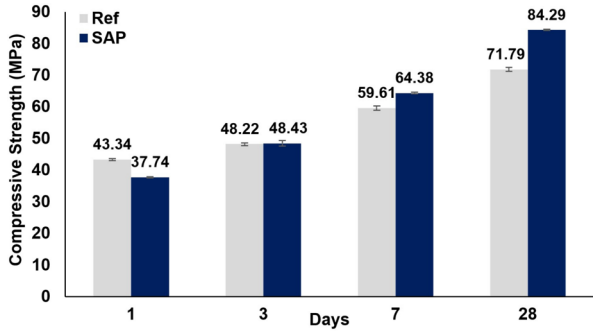

Figure 1. Compressive strength.

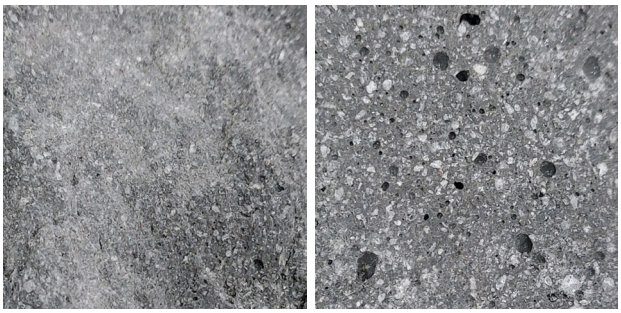

(a) Ref (b) SAP

Figure 2. Failure area of 28 days specimen.

3.2. Estimation of cement hydration by image processing

The X-Ray μCT image represents material density, scaled in grayscale values ranging from 0 to 255. Each pixel's grayscale value is recorded and plotted, as shown in Figure 3. As hydration occur and density increases over time (39), the grayscale value distribution shifts towards the right. In the case of Ref-specimens, there is a notable increase in hydration from day 1 to 3, indicating a significant shift in the grayscale value distribution. On the other hand, SAP-specimens occurs from day 7 to 28. These results align with the compressive strength test as shown in Figure 1. These results uncovered the phenomenon of slow rate hydration at day 1 to 3, as evidenced by the compressive strength between days 1 and 3, which has yet to be explored in previous studies.

Figure 4 shows greyscale value distributions of the Ref- and SAP-specimens for both the outer and inner (core) specimens. The Ref-specimen exhibits a peak grayscale value of 96 for the outer part and 93 for the inner part, while

the SAP-specimen shows identical peak grayscale values of 96 for both outer and inner regions. It should be note that in image analysis, the greater value of GSV shows the higher density of matrix. Subsequently, the similarity in these values implies comparable degrees of hydration on the outer and inner portions, indicating the effectiveness of SAP as an internal curing medium results in uniform hydration along the specimen.

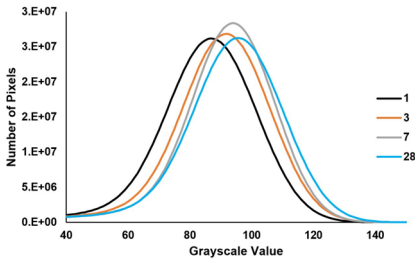

(a) Ref

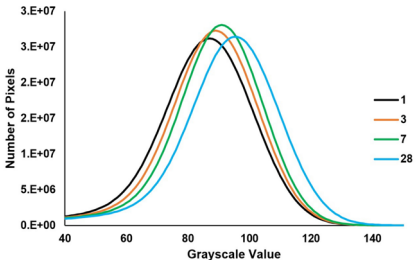

(b) SAP

Figure 3. Greyscale value distribution within the range of 40 to 140.

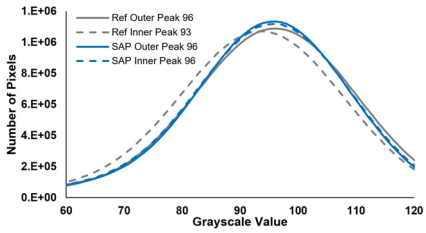

Figure 4. GSV distribution for inner and outer part of Ref- and SAP-specimen.

3.3. Porosity

The porosity in this study is presented in Figure 5. The use of SAP in the mixture increases the porosity at all ages. Up to 28 days, the difference in porosity was 0.68%. Previous study found that adding SAP does not significantly impact porosity as long as the total water-to-cement ratio (w/c) remains constant (5). This increase in porosity can be attributed to the density of SAP, which is closer to that of air than that of the matrix. Consequently, the void calculations carried out using X-Ray µCT indicated a potential contribution from SAP as macro pores, particularly when considering SAP sizes ranging from 100-200 µm.

Porosity testing was also conducted using water penetration (ASTM C642) to validate the results obtained from X-ray µCT. Figure 6 shows the volume of permeable void (VPV) for both specimens. From Figure 6, it can be seen that Ref-specimen was 5.61%, while for the SAP-specimen, it was 5.88%. It's noteworthy that the VPV values in both specimens exceed those of the X-Ray µCT approach. The accuracy of X-Ray µCT outcomes is reliant on the resolution employed, which in this study was 26 µm. As a result, pores smaller than 26 µm remain undetectable, leading to an underestimation of the quantified porosity results.

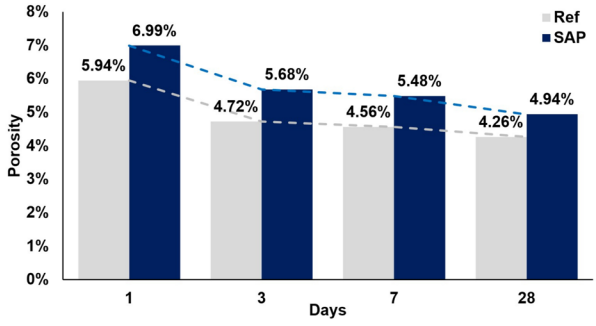

Figure 5. Porosity of X-Ray µCT.

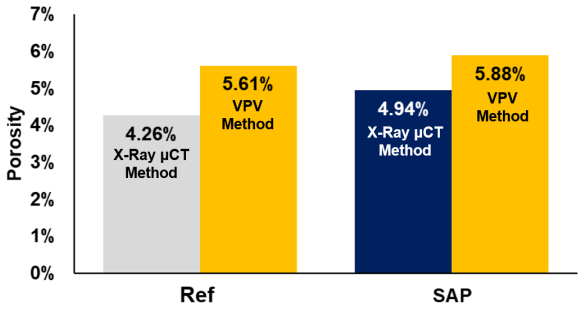

Figure 6. Porosity of X-Ray µCT and VPV at 28 days.

3.4. Pore size distribution

Figure 7 shows the pore size evolution for both Ref-specimen (Figure 7a) and SAP-specimen (Figure 7b). A significant decrease in the number of pores is observed in Ref-specimen from days 1 to 3, while for SAP-specimen, the decrease occurs from days 3 to 7. The slow decrease in pores for SAP-specimens can be attributed to the absorption of water by SAP during the early stages. However, there is a significant reduction in pore size at later stages, particularly for pores of similar size to SAP particles.

The change in pore size for SAP specimens can be evaluated by observing SAP particles evolution in the matrix with time. Figure 8 shows the size evolution of SAP-pores. As shown in Figure 8, SAP particles are sometimes attached and contribute to the pore size. The pores formed by the release of water provide space for the accumulation of hydration products (40). In this regard larger voids are observed to decrease in size (41).

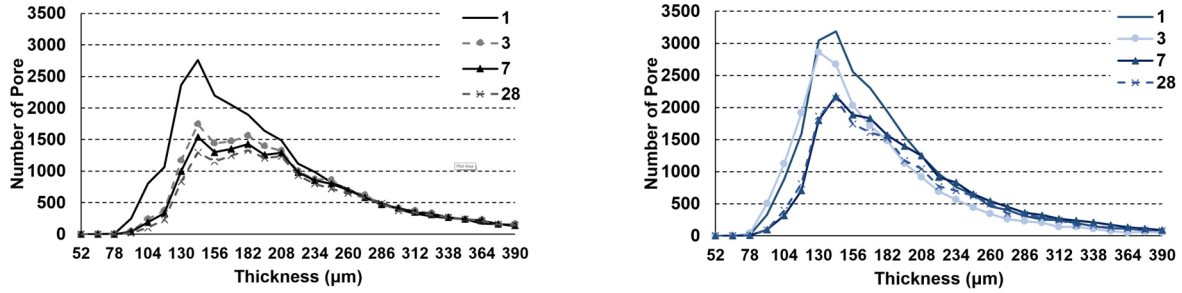

(a) Ref (b) SAP

Figure 7. Pore size distribution evolution at 1, 3, 7, and 28 days.

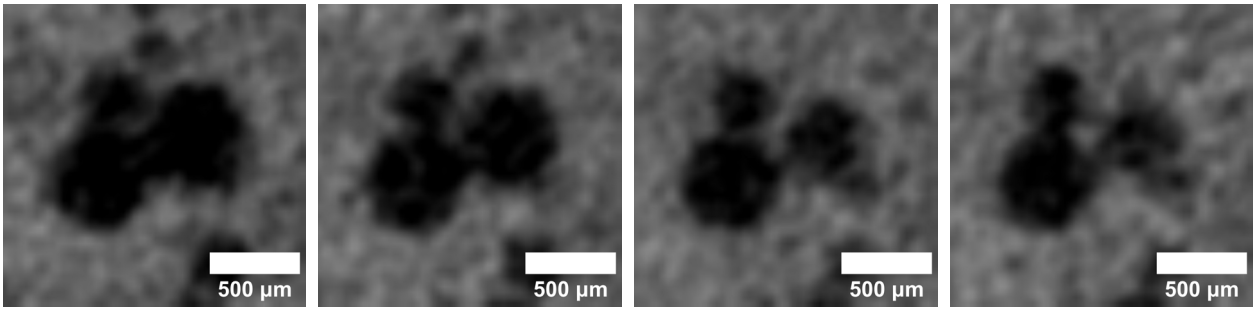

(a) 1 days (b) 3 days (c) 7 days (d) 7 days

Figure 8. Pore evolution in 2D image.

3.5. Pore shape

The sphericity of Ref-specimens demonstrates a consistent tendency, with a value of 0.7 comprising 77% of the occurrences, thus fitting the category of moderate sphericity. In contrast, the sphericity of SAP-specimens, also bearing a value of 0.7, only accounts for 58% due to a more dispersed distribution spanning sphericities of 0.6 and 0.5, leading to its classification as having low sphericity (28). It is estimated that SAP-pore contributed to the sphericity of total pore in SAP-specimen. Dry SAP particles tend to have a round shape and a specific density, but when saturated with water, the SAP particles change into a hydrogel form. Therefore, in the hydrogel form, the elasticity of the SAP particles increases, and the shape of the hydrogel is easily changed through the compaction process during casting and the water release process.

3.6. The presence of SAP

The detection of superabsorbent polymer (SAP) within the microstructure of cement-based materials has been demonstrated through SEM backscattered electron, enabling the identification of SAP voids and collapsed SAP (42). Nevertheless, as previously discussed, utilizing SEM for image acquisition has limitations. Hence, a more accurate observation of the microstructure image of SAP in cement-based materials necessitates the utilization of X-Ray μCT.

Figure 9 illustrates several phases captured through X-Ray μCT. Qualitatively, two distinct voids are observable, including completely black voids and voids filled with a dark gray substance, which signifies presoaked SAP with tracer potassium iodide. Quantitative analysis can detect the presence of the SAP-tracer through the line profile.

Figure 10 indicates that air voids have an almost negligible grayscale value inside, mainly due to their composition of air. In contrast, SAP-tracer voids exhibit a discernible entity at the center, represented as SAP particles. This observation strongly supports to the classification of SAP as a void in the porosity analysis conducted via the X-Ray μCT method. It also validates SAP's impact on pore characteristics, particularly regarding sphericity.

The evolution of SAP within cement-based materials can also be observed by conducting scans at 1, 3, and 7 days. An example of SAP voids was analyzed using a Volume of Interest (VOI) measuring 120×120×60 voxels, as shown in Figure 11, which presents slices of the SAP void at various heights. The void was segmented into 60 horizontal slices, similar to the Earth's latitudinal divisions. The analysis specifically focuses on the 15th, 30th (center), and 45th slices to provide a representative view of the void's internal structure at different heights.

Depending on the observation height, SAP particles exhibit two distinct forms in the imaging. Close to the surface, the SAP image appears as complete circles (Z=15 and Z=45), while at the center (Z=30), it forms a ring-like shape. Performing a 3D scan explains the two types of SAP shapes in the previous study using SEM (42).

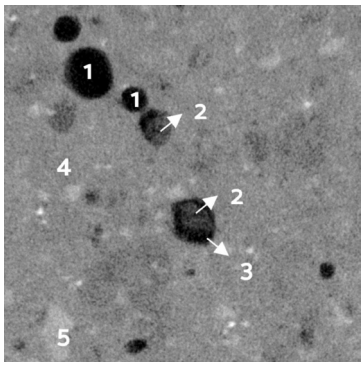

(a) Air void.

Figure 9. Microstructure phase: (1) Air void; (2) SAP particle; (3) SAP void; (4) Matrix; (5) Aggregate.

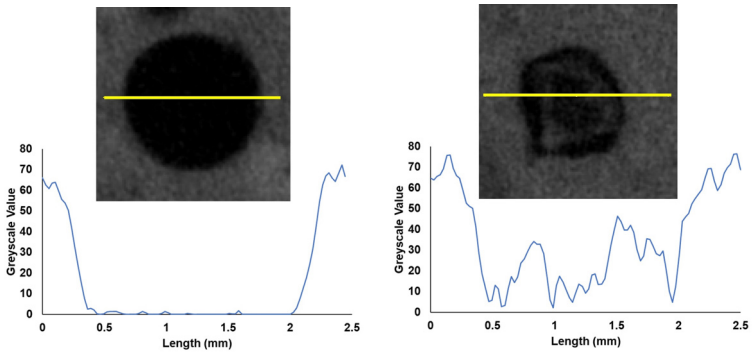

(b) SAP-tracer void.

Figure 10. Greyscale value of line profile at the center of void.

Slices	Day 1	Day 3	Day 7
Z=15	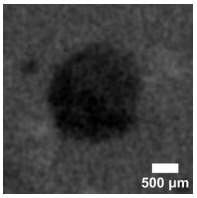	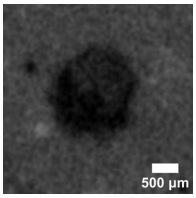	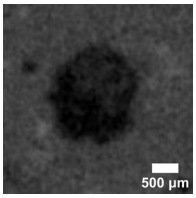
Z=30	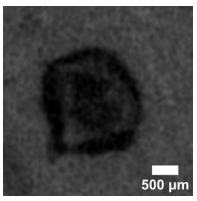	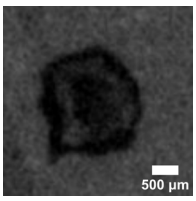	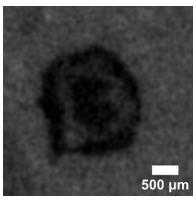
Z=45	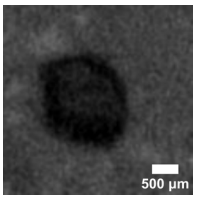	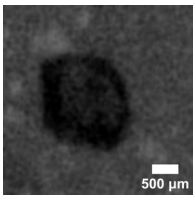	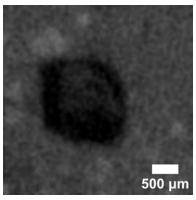

Figure 11. The evolution of SAP at various height.

Figure 11 also illustrates the evolution of SAP over time. At Z=15, it can be observed that initially, it attaches to the matrix, but over time, it becomes more separated due to the shrinking of SAP as it releases previously absorbed water. At Z=30, the boundaries of the SAP ring gradually become less distinct. This change is quantified through the line profile, as shown in Figure 12. From Figure 12, it can be seen that the center of the SAP exhibits a diminishing grayscale value as time progresses. This change can be attributed to the release of the tracer by the SAP.

Consequently, X-Ray µCT scanning of SAP provides a clearer view of the physical conditions within the voids, offering a more comprehensive 3D understanding of SAP void structure. It also confirms that SAP contributes to calculated porosity in X-Ray µCT methods and impacts the resulting pore shape.

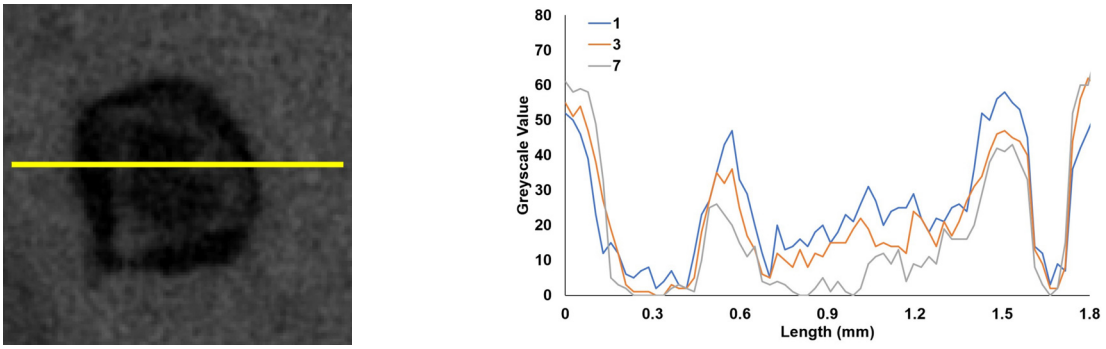

Figure 12. Greyscale value of line profile at inner SAP void at 1, 3, and 7 days.

3.7. The dispersion of SAP

Figure 13 shows the increased grayscale value in the line profile for the outer SAP void at 1, 3, and 7 days. The line profile analysis shows the enhancement in grayscale value in the outer SAP void. There is a significant increase from day 1 to day 3, while the increase from day 3 to day 7 is relatively small, which can be attributed to the water-to-cement ratio (w/c) of 0.5, allowing for faster densification and reduced effectiveness of internal curing from SAP (43).

According to the line profile, SAP's internal curing effective range is around 30 pixels or 0.9 mm. Previous study found that SAP can release water up to a distance of 2-3 mm in the early stages, calculated numerically (44). Nevertheless, the densification in the capillary pores will progressively reduce the supply range, making the effective range shorter over time. However, it should be not that the effect of the tracer solution on the hydration of cement remains unknown although the distance of released tracer can provide valuable insight regarding the behavior of the SAP embedded in the cement hydration products.

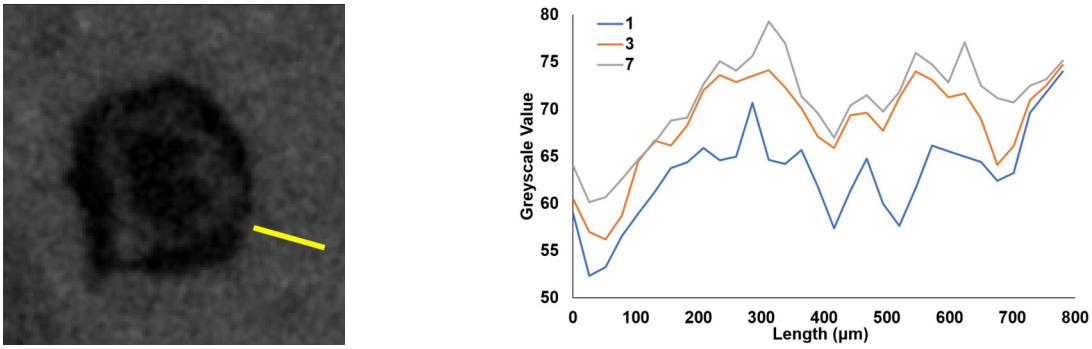

Figure 13. Greyscale value of line profile at outer SAP void at 1, 3, and 7 days.

3.8. Crack geometry parameters

Table 3 shows the crack geometry parameters for Ref- and SAP-specimens after extracting the crack from the CT images. The tortuosity for Ref- and SAP-specimens are found to be around 1.10 and 1.04, respectively. Darma et al. (2013) (16) reported that for the specimen which contains maximum aggregate size of 1.7 mm, w/c ratio of 0.6 and crack was induced by splitting tensile test, the length of crack was about 25% longer that the length of specimen. This result implies that in the same crack inducing method, the tortuosity depends on the mix proportion as well as maximum aggregate size.

Table 3. Crack geometry parameters.

Spesimen	Residual Crack Width (μm)	Tortuosity	Mean Crack Width (μm)	Constrictivity
Ref	216	1.10	227.89	0.58
SAP	238	1.04	247.17	0.71

Figure 14 shows the crack width distribution for both specimens. Ref-specimen has a more extensive crack width distribution, reflecting the higher variation of crack width along the crack length. Large differences in crack width

significantly affect the lower degree of constrictivity. The constrictivity of SAP-specimen is larger than that of Ref-specimen, although the residual crack opening width of Ref-specimen is smaller than that of SAP-specimen. Darma et al. (2013) (15) showed that the use of fly ash increased the constrictivity of crack. Pozzolanic reaction products creating a more densified material. In this regard the propagation of cracks is expected to occurs in the area around the aggregate and cement matrix resulting to a more uniform crack width.

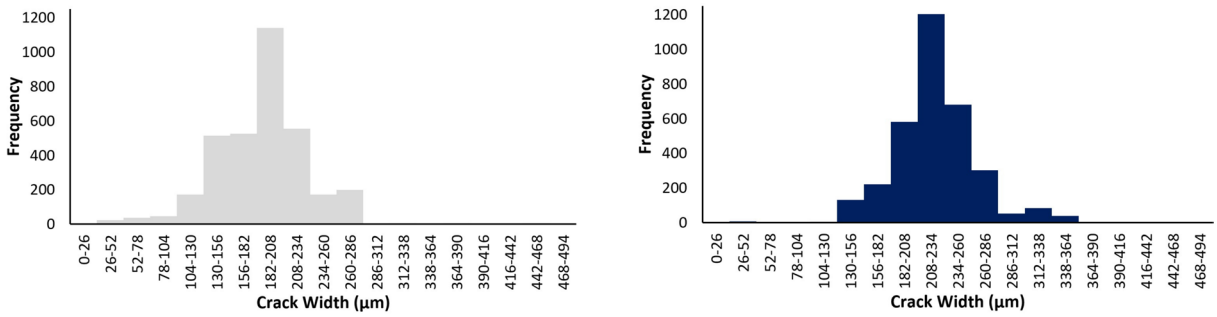

(a) Ref (b) SAP

Figure 14. Crack width distribution.

Fly ash contributes to increased cement based materials density through pozzolanic reactions. In this study, the incorporation of SAP in low water-to-cement ratios, serving as internal curing, enhances the degree of hydration, resulting in a lower amount of unhydrated cement grains.

3.9. Capillary absorption

Figure 15 shows tracer penetration in Ref- and SAP-specimens. The tracer makes the penetrated specimen brighter. The height of penetration can be obtained from 3D orthogonal slice. While tracer penetration is visible from the bottom surface, distinguishing the difference between Ref- and SAP-specimens is challenging, and determining the penetration height becomes subjective. Enhancing the contrast can make the tracer penetration boundary more visible. One of the existing quantitative methods is using line profile and analyzing the difference in greyscale value trendlines (29), ilustrated in Figure 16.

Based on the line profile analysis, the penetration depths of the Ref-specimen and SAP specimen were 1.53 mm and 1.62 mm, respectively. The capillary coefficient was calculated and the results are presented in Table 4. The apparent coefficients obtained in this study are considered reasonable and are within reported ranges by previous research (45). However, in comparison to a previous study that also using image quantitative method, a difference of two orders of magnitude is observed. This discrepancy can be reasonably explained by the lower w/c used in the present study, as a lower w/c ratio generally leads to lower total pores resulting in smaller penetration depths.

This result implies that Ref-specimen and SAP-specimen has similar water penetration depth through the uncracked surface. It is expected that up to several depth from the specimen surface the hydration level are same under the same curing condition.

Table 4. Capillary coefficient.

Specimen		w/c	Capillary Coefficient ($m/s^{1/2}$)	SAP Addition	Method
Ref		0.20	5.21×10^{-6}	Without SAP	X-Ray μCT
SAP		0.20	5.51×10^{-6}	With SAP	X-Ray μCT
Previous Study	(44)	0.20	2.31×10^{-6}	Without SAP	Additional weight
	(45)	0.40	1.15×10^{-4}	Without SAP	Neutron radiography
	(25)	0.45	1.65×10^{-4}	Without SAP	X-Ray CT

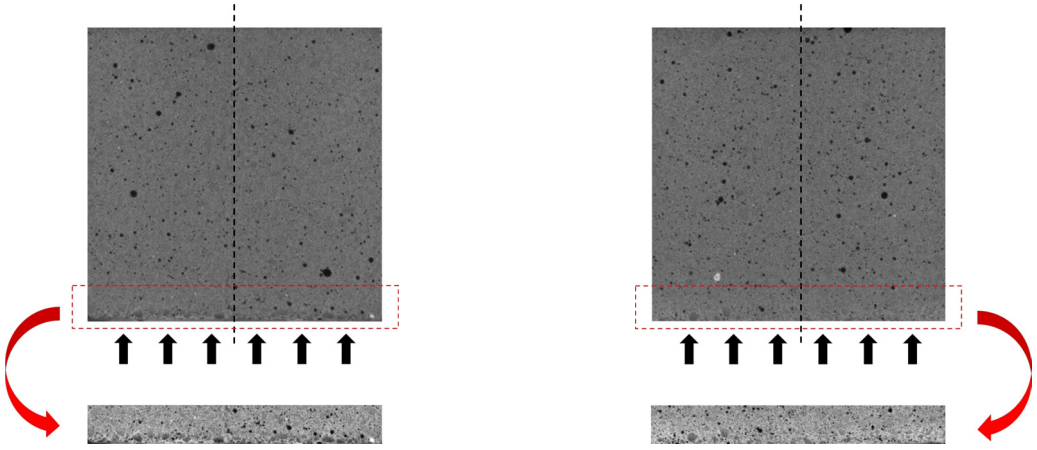

(a) Ref (b) SAP

Figure 15. Orthogonal slice capillary absorption.

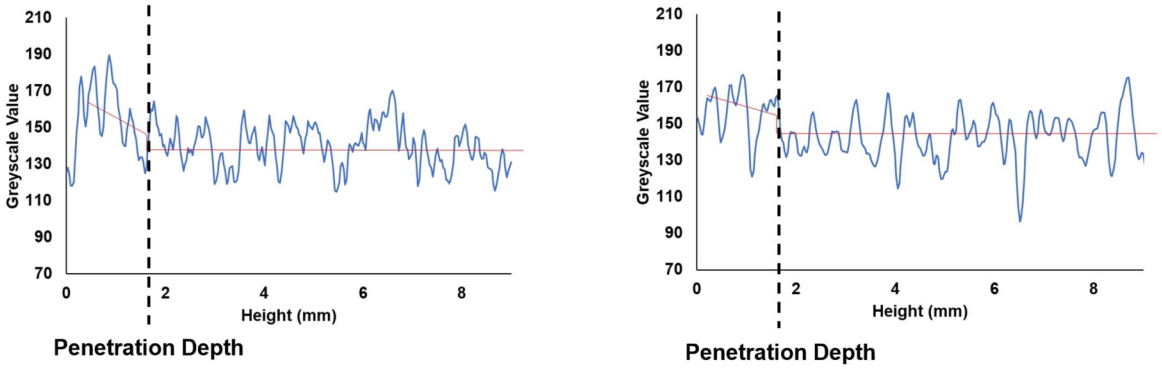

(a) Ref (b) SAP

Figure 16. Greyscale value line profile capillary absorption.

3.10. Capillary absorption throgh crack

Figure 17 shows the maximum lateral penetration through cracks in both Ref- and SAP-specimens, it can be seen that penetration of tracer in uncracked body for SAP specimens is lower than that of Ref-specimens. Figure 18 shows the line profile analysis for quantification of tracer penetration depth. The depth penetration, of the Ref-specimen and SAP specimen were found to be around 3.95 mm and 1.45 mm, respectively. This implies that the Ref-specimen's penetration was approximately 2.7 times deeper than SAP-specimen. This difference can be attributed to the densification effect on matrix and capillary pores for SAP-specimens. These findings further support that SAP can serve as an internal curing medium and preventing the presence of unhydrated cement as shown in Figure 2.

The penetration height of the tracer in capillary absorption through crack can also be assessed through a 3D analysis, as shown in Figure 19. It can be seen that the penetration of Ref-specimens is deeper towards both sides, which is characterized by thicker segmentation results.

As shown in Tabel 4 the capillary coefficient uncracked surface of Ref-specimens is similar with that of SAP-specimens. However, for the case of capillary absorption through cracks, the difference in penetration depth is significantly distinct of equivalent crack opening width.

There is no previous study has analyzed the transport properties of Ref- and SAP-specimens using X-Ray μCT and capillary absorption. To confirm the densification formed can be through comparison with RCPT or carbonation testing in previous studies, although there are drawbacks of these tests. The previous study also found that transport properties would decrease when using SAP (5, 47).

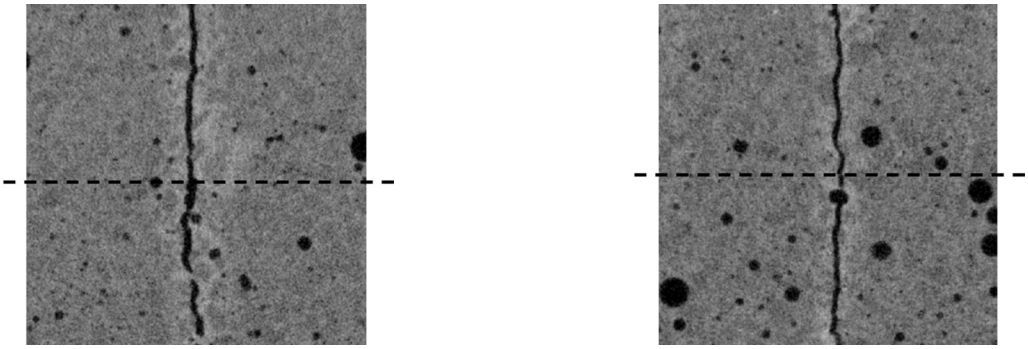

(a) Ref (b) SAP

Figure 17. Orthogonal slice capillary absorption through crack.

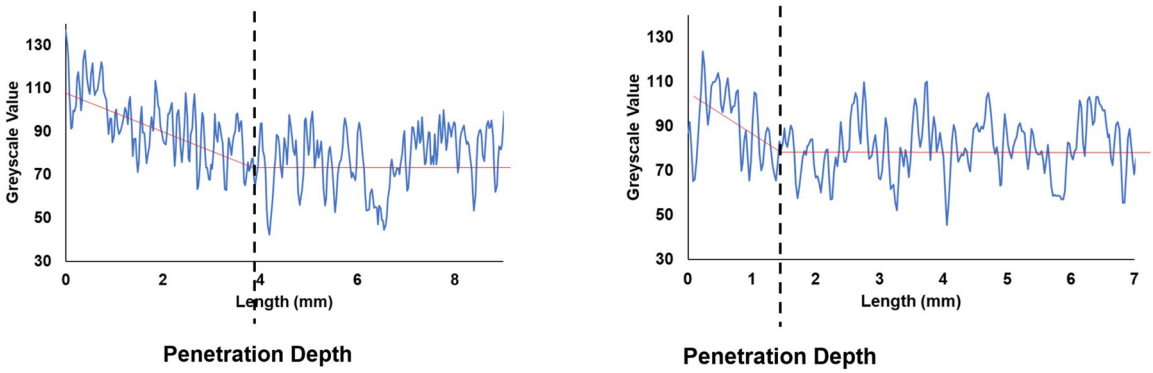

(a) Ref (b) SAP

Figure 18. Greyscale value line profile capillary absorption through crack.

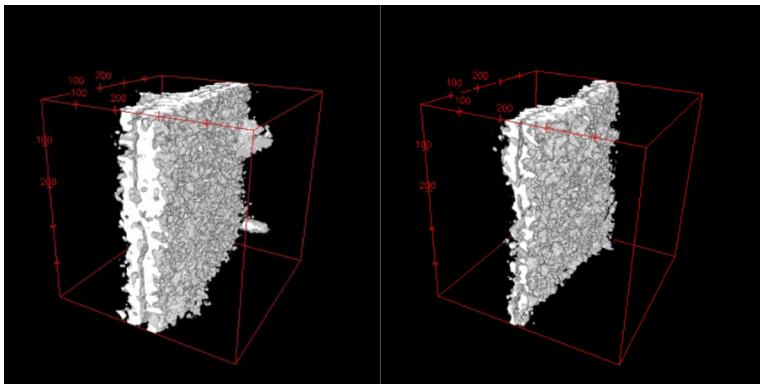

(a) Ref (b) SAP

Figure 19. 3D tracer penetration through crack.

In mortar with a low w/c ratio, the conventional curing by water immersion is only effective for several depth from the surface neither spesimens core. Water penetration during the curing process may not reach the core of the mortar, leading to a lower degree of hydration leaving a high presence of unhydrated cement grains. In contrast to SAP specimens, the water supply from SAP facilitating the hydration process in the core even in very low water conditions.

These test results imply that SAP, as an internal curing agent, contributes to achieving a higher final degree of hydration, resulting in better density and consequently lower capillary coefficient values. On a laboratory scale, spesimens incorporating SAP (with the same water content, cement content, w/c ratio, and mixing method) has demonstrated improvements in quality and durability, suggesting potential cost savings for industrial applications. However, further exploration is required, as the distribution of SAP during mixing poses a challenge. Full-scale testing may be necessary to fully understand and optimize SAP dispersion in practical construction settings.

4. CONCLUSIONS

Based on this study, the following conclusions are drawn.

1. The addition of SAP increase for both degree and uniformity of hydration in low w/c cementitious materials resulted in increasing compressive strength by 17.4%.
2. SAP does not impact total porosity; it does affect pore structure size by decreasing peak pore thickness by 15% and did not cause increased of percolated voids.
3. The presence of SAP induces densification within capillary pores by releasing supply water up to 0.9 mm outside the voids.
4. In swollen state, SAP particle appears as complete circle at close to the surface and ring-like shape in the center.
5. In the same crack inducing method, the tortuosity of crack depends on the mix proportion as well as maximum aggregate size. The addition SAP increased the crack width uniformity.
6. Capillary absorption coefficients of concrete with SAP are similar for both cracked and uncracked bodies. The absence of SAP results in 2.7 times greater penetration for the core than that of the surface in normal mortar.
7. X-Ray μCT demonstrates efficacy in microstructure analysis and assessing the durability of cement-based materials.

Acknowledgements

Part of this research was funded by Structural Engineering Research Group, Faculty of Civil and Environmental Engineering, Bandung Institute of Technology, Indonesia. The author also gratefully acknowledges the support from the Structural Engineering Laboratory and Basic Science Center A Laboratory in Bandung Institute of Technology.

Authorship contribution statement

Abdurrahman Yusuf: Conceptualization, Formal analysis, Writing-original draft.
Ivan Sandi Darma: Conceptualization, Supervision, Methodology, Writing-review & editing.
Ediansjah Zulkifli: Data Curation, Supervision, Writing-review & editing.
Rani Pradoto: Data Curation, Supervision, Writing-review & editing.

Declaration of competing interest

The authors of this article declare that they have no financial, professional or personal conflicts of in-terest that could have inappropriately influenced this work.

REFERENCES

1. Kumar Mehta P, Monteiro PJM. 2014. Concrete: microstructure, properties, and materials, Fourth Edition.
2. Schröfl C, Snoeck D, Mechtcherine V. 2017. A review of characterisation methods for superabsorbent polymer (SAP) samples to be used in cement-based construction materials: report of the RILEM TC 260-RSC. Materials and Structures/Materiaux et Constructions. 50:197. https://doi.org/10.1617/s11527-017-1060-4
3. Miller AE, Barrett TJ, Weiss WJ. 2014a. Evaluation of superabsorbent polymers for use in cementitious systems for the purpose of mitigating autogenous shrinkage. International RILEM Conference on Application of Superabsorbent Polymers and other New Admixtures in Concrete Construction.
4. Mechtcherine V, Wyrzykowski M, Schröfl C, Snoeck D, Lura P, de Belie N, Mignon A, van Vlierberghe S, Klemm AJ, Almeida FCR, et al. 2021. Application of super absorbent polymers (SAP) in concrete construction—update of RILEM state-of-the-art report. Materials and Structures/Materiaux et Constructions. 54:80. https://doi.org/10.1617/s11527-021-01668-z
5. Beushausen H, Gillmer M, Alexander M. 2014. The influence of superabsorbent polymers on strength and durability properties of blended cement mortars. Cem Concr. Compos. 52: 73-80. https://doi.org/10.1016/j.cemconcomp.2014.03.008
6. Justs J, Wyrzykowski M, Winnefeld F, Bajare D, Lura P. 2014. Influence of superabsorbent polymers on hydration of cement pastes with low water-to-binder ratio: A calorimetry study. J. Therm. Anal. Calorim. 115:425–432. https://doi.org/10.1007/s10973-013-3359-x
7. Guo Y, Zhang P, Ding H, Le C. 2020. Experimental study on the permeability of SAP modified concrete. Materials. 13(15):3368. https://doi.org/10.3390/ma13153368
8. Dang J, Zhao J, Du Z. 2017. Effect of superabsorbent polymer on the properties of concrete. Polymers (Basel). 9(12):672. https://doi.org/10.3390/polym9120672

9. Farzanian K, Pimenta Teixeira K, Perdigão Rocha I, De Sa Carneiro L, Ghahremaninezhad A. 2016. The mechanical strength, degree of hydration, and electrical resistivity of cement pastes modified with superabsorbent polymers. Constr. Build. Mater. 109:156-165. https://doi.org/10.1016/j.conbuildmat.2015.12.082
10. Reinhardt HW, Assmann A. 2009. Enhanced durability of concrete by superabsorbent polymers. In: Brittle Matrix Composites 9.
11. Zhang Y, Yang B, Yang Z, Ye G. 2019. Ink-bottle effect and pore size distribution of cementitious materials identified by pressurization-depressurization cycling mercury intrusion porosimetry. Materials. 12(9):1454. https://doi.org/10.3390/ma12091454
12. Wang X, Peng Y, Wang J, Zeng Q. 2019. Pore structure damages in cement-based materials by mercury intrusion: A non-destructive assessment by X-ray computed tomography. Materials. 12(14):2220. https://doi.org/10.3390/ma12142220
13. Bartoš M, Suchý T, Foltán R. 2018. Note on the use of different approaches to determine the pore sizes of tissue engineering scaffolds: What do we measure? Biomed Eng Online. 17:110. https://doi.org/10.1186/s12938-018-0543-z
14. Chung SY, Kim JS, Stephan D, Han TS. 2019a. Overview of the use of micro-computed tomography (micro-CT) to investigate the relation between the material characteristics and properties of cement-based materials. Constr. Build. Mater. 229:116843. https://doi.org/10.1016/j.conbuildmat.2019.116843
15. du Plessis A, Boshoff WP. 2019. A review of X-ray computed tomography of concrete and asphalt construction materials. Constr. Build. Mater. 199:637-651. https://doi.org/10.1016/j.conbuildmat.2018.12.049
16. Darma IS, Sugiyama T, Promentilla MAB. 2013. Application of X-ray CT to study diffusivity in cracked concrete through the observation of tracer transport. J. Adv. Concr. Technol. 11(10):266-281. https://doi.org/10.3151/jact.11.266
17. Yang L, Zhang Y, Liu Z, Zhao P, Liu C. 2015. In-situ tracking of water transport in cement paste using X-ray computed tomography combined with CsCl enhancing. Mater Lett. 160:381-383. https://doi.org/10.1016/j.matlet.2015.08.011
18. Liu Z, Wang J, Zhang Y, Lv H, Fu P, Li A. 2017. In situ characterisation of the depth and mass of water intrusion in unsaturated cement pastes via X-ray computed tomography. Adv. Cem. Res. 29(3):91–100. https://doi.org/10.1680/jadcr.16.00056
19. Sumra Y, Payam S, Zainah I. 2020. The pH of cement-based materials: a review. Journal Wuhan University of Technology, Materials Science Edition. 35:908–924. https://doi.org/10.1007/s11595-020-2337-y
20. Huang X, Liu X, Rong H, Yang X, Duan Y, Ren T. 2022. Effect of Super-Absorbent Polymer (SAP) incorporation method on mechanical and shrinkage properties of internally cured concrete. Materials. 15(21):7854. https://doi.org/10.3390/ma15217854
21. Ritschl L, Bergner F, Fleischmann C, Kachelrie M. 2010. Water calibration for CT scanners with tube voltage modulation. Phys. Med. Biol. 55:4107. https://doi.org/10.1088/0031-9155/55/14/010
22. Chung SY, Kim JS, Stephan D, Han TS. 2019. Overview of the use of micro-computed tomography (micro-CT) to investigate the relation between the material characteristics and properties of cement-based materials. Constr. Build. Mater. 229:116843. https://doi.org/10.1016/j.conbuildmat.2019.116843
23. Kim JS, Chung SY, Stephan D, Han TS. 2019. Issues on characterization of cement paste microstructures from μ-CT and virtual experiment framework for evaluating mechanical properties. Constr. Build. Mater. 202:82-10. https://doi.org/10.1016/j.conbuildmat.2019.01.030
24. Lawrence TJ, Carr SJ, Manning AJ, Wheatland JAT, Bushby AJ, Spencer KL. 2023. A novel 3D volumetric method for directly quantifying porosity and pore space morphology in flocculated suspended sediments. MethodsX. 10:101975. https://doi.org/10.1016/j.mex.2022.101975
25. Hildebrand T, Rüegsegger P. 1997. A new method for the model-independent assessment of thickness in three-dimensional images. J Microsc. 185(1):67-75. https://doi.org/10.1046/j.1365-2818.1997.1340694.x
26. Dougherty R, Kunzelmann KH. 2007. Computing local thickness of 3d structures with image. J. Microscopy and Microanalysis. 13(S02):1678–1679. https://doi.org/10.1017/s1431927607074430
27. Doube M, Kłosowski MM, Arganda-Carreras I, Fabrice P.C., et al. 2010. BoneJ : free and extensible bone image analysis in ImageJ. Bone. 47(6):1076-1079. https://doi.org/10.1016/j.bone.2010.08.023
28. Tamura Y, Busby CJ, Blum P, Guèrin G, Andrews GDM, Barker AK, Berger JLR, Bongiolo EM, Bordiga M, DeBari SM, et al. 2015. Expedition 350 methods. Proceedings of the International Ocean Discovery Program. 350 https://doi.org/10.14379/iodp.proc.350.102.2015
29. Yang L, Gao D, Zhang Y, Tang J, Li Y. 2019. Relationship between sorptivity and capillary coefficient for water absorption of cement-based materials: Theory analysis and experiment. R. Soc. Open Sci. 6:190112. https://doi.org/10.1098/rsos.190112
30. Mohammad M, Tariq M, Qadri MS, Latif M, Tahiri IA, Naz L. 2015. Diffusion coefficient of iodide ions in aqueous medium and in vacuum: An appraisal. J. Chem. Soc. Pak. 37(6):440. Retrieved from https://jcsp.org.pk/issueDetail.aspx?aid=b001bc19-fda3-4716-8278-b749feab5f0a
31. Khanzadeh Moradllo M, Hu Q, Ley MT. 2017. Using X-ray imaging to investigate in-situ ion diffusion in cementitious materials. Constr. Build. Mater. 136:88-98. https://doi.org/10.1016/j.conbuildmat.2017.01.038
32. Arganda-Carreras I, Fernández-González R, Muñoz-Barrutia A, Ortiz-De-Solorzano C. 2010. 3D reconstruction of histological sections: Application to mammary gland tissue. Microsc. Res. Tech. 73(11):1019-1029. https://doi.org/10.1002/jemt.20829
33. Evans RB, Watson GM, Mason EA. 1961. Gaseous diffusion in porous media at uniform pressure. J. Chem. Phys. 35:2076–2083. https://doi.org/10.1063/1.1732211
34. Al-Nasra M, Daoud M. 2017. Study of the ability of cracked concrete to block water flow, concrete mixed with super absorbent polymer. ARPN J. Eng. Appl. Sci. 12(1).

35. Ma X, Liu J, Wu Z, Shi C. 2017. Effects of SAP on the properties and pore structure of high performance cement-based materials. Constr. Build. Mater. 131:476-484. https://doi.org/10.1016/j.conbuildmat.2016.11.090
36. Miller AE, Barrett TJ, Weiss WJ. 2014. Evaluation of superabsorbent polymers for use in cementitious systems for the purpose of mitigating autogenous shrinkage. International RILEM Conference on Application of Superabsorbent Polymers and other New Admixtures in Concrete Construction.
37. Mechtcherine V, Wyrzykowski M, Schröfl C, Snoeck D, Lura P, De Belie N, Mignon A, Van Vlierberghe S, Klemm AJ, Almeida FCR, et al. 2021. Application of super absorbent polymers (SAP) in concrete construction—update of RILEM state-of-the-art report. Materials and Structures/Materiaux et Constructions. 54:80. https://doi.org/10.1617/s11527-021-01668-z
38. Suleiman AR, Zhang L V., Nehdi ML. 2021. Quantifying crack self-healing in concrete with superabsorbent polymers under varying temperature and relative humidity. Sustainability. 13(24):13999. https://doi.org/10.3390/su132413999
39. Opara HE, Eziefula UG, Eziefula BI. 2018. Comparison of physical and mechanical properties of river sand concrete with quarry dust concrete. Selected Scientific Papers - Journal of Civil Engineering. 13(s1):127-134. https://doi.org/10.1515/sspjce-2018-0012
40. Lu Y, Wang K, Zhu D, Meng Q, Cui L. 2022. Hydration and pore structure characteristics of concrete incorporating internal curing materials in a dry and largeerature-difference environment. Mater. Res. Express. 9:035502. https://doi.org/10.1088/2053-1591/ac5a31
41. Moradian M, Hu Q, Aboustait M, Ley MT, Hanan JC, Xiao X, Scherer GW, Zhang Z. 2017. Direct observation of void evolution during cement hydration. Mater. Des. 136:137-149. https://doi.org/10.1016/j.matdes.2017.09.056
42. Wong HS. 2018. Concrete with superabsorbent polymer. In: Eco-efficient repair and rehabilitation of concrete infrastructures. 2018:467-499. https://doi.org/10.1016/B978-0-08-102181-1.00017-4
43. Schroefl C, Mechtcherine V, Vontobel P, Hovind J, Lehmann E. 2015. Sorption kinetics of superabsorbent polymers (SAPs) in fresh Portland cement-based pastes visualized and quantified by neutron radiography and correlated to the progress of cement hydration. Cem. Concr. Res. 75:1-13. https://doi.org/10.1016/j.cemconres.2015.05.001
44. Wyrzykowski M, Lura P, Pesavento F, Gawin D. 2012. Modeling of water migration during internal curing with superabsorbent polymers. J. Mater. Civ. Eng. 24(8). https://doi.org/10.1061/(asce)mt.1943-5533.0000448
45. Ma H, Wang P, Zhao T, Du Z, Zhao L. 2017. Influence of W/C and moisture content on capillary adsorption of concrete. DEStech Transac. Mater. Sci. Engin. https://doi.org/10.12783/dtmse/ictim2017/9928
46. Zhang P, Wittmann FH, Zhao TJ. 2011. Quantitative determination of capillary absorption of concrete. Basic Research on Concrete and Applications
47. Wehbe Y, Ghahremaninezhad A. 2017. Combined effect of shrinkage reducing admixtures (SRA) and superabsorbent polymers (SAP) on the autogenous shrinkage, hydration and properties of cementitious materials. Constr. Build. Mater. 138:151-162. https://doi.org/10.1016/j.conbuildmat.2016.12.206